THE JOURNAL OF BIOLOGICAL CHEMISTRY VOL. 283, NO. 12, pp. 7912–7920, March 21, 2008

A Structural-Dynamical Characterization of Human Cox17*[S]

Received for publication, September 25, 2007, and in revised form, November 26, 2007 Published, JBC Papers in Press, December 19, 2007, DOI 10.1074/jbc.M708016200

Lucia Banci[‡], Ivano Bertini[‡1], Simone Ciofi-Baffoni[‡], Anna Janicka[‡§], Manuele Martinelli[‡], Henryk Kozlowski[§], and Peep Palumaa[¶]

From the [‡]Magnetic Resonance Center Centro Risonanze Magnetiche (CERM) and Department of Chemistry, University of Florence, Via Luigi Sacconi 6, 50019, Sesto Fiorentino, Florence, Italy, the [§]Faculty of Chemistry, University of Wroclaw, F. Joliot-Curie 14, 50383 Wroclaw, Poland, and the [¶]Department of Gene Technology, Tallinn University of Technology, Akadeemia tee 15, 12618 Tallinn, Estonia

Human Cox17 is a key mitochondrial copper chaperone responsible for supplying copper ions, through the assistance of Sco1, Sco2, and Cox11, to cytochrome *c* oxidase, the terminal enzyme of the mitochondrial energy transducing respiratory chain. A structural and dynamical characterization of human Cox17 in its various functional metallated and redox states is presented here. The NMR solution structure of the partially oxidized Cox17 ($Cox17_{2S\text{-}S}$) consists of a coiled coil-helix-coiled coil-helix domain stabilized by two disulfide bonds involving Cys^{25}–Cys^{54} and Cys^{35}–Cys^{44}, preceded by a flexible and completely unstructured N-terminal tail. In human Cu(I)$Cox17_{2S\text{-}S}$ the copper(I) ion is coordinated by the sulfurs of Cys^{22} and Cys^{23}, and this is the first example of a Cys-Cys binding motif in copper proteins. Copper(I) binding as well as the formation of a third disulfide involving Cys^{22} and Cys^{23} cause structural and dynamical changes only restricted to the metal-binding region. Redox properties of the disulfides of human Cox17, here investigated, strongly support the current hypothesis that the unstructured fully reduced Cox17 protein is present in the cytoplasm and enters the intermembrane space (IMS) where is then oxidized by Mia40 to $Cox17_{2S\text{-}S}$, thus becoming partially structured and trapped into the IMS. $Cox17_{2S\text{-}S}$ is the functional species in the IMS, it can bind only one copper(I) ion and is then ready to enter the pathway of copper delivery to cytochrome *c* oxidase. The copper(I) form of $Cox17_{2S\text{-}S}$ has features specific for copper chaperones.

Eukaryotic cytochrome *c* oxidase (CcO),[2] the terminal enzyme of the energy transducing respiratory chain of cells, is embedded within the mitochondrial inner membrane with a portion of the molecule protruding into the intermembrane space (IMS) (37 Å) and a portion extending into the matrix (32 Å) (1, 2). Mammalian CcO is composed of 13 subunits, and its assembly is dependent on the insertion of several cofactors necessary for function, including two hemes, three copper ions, zinc, magnesium, and sodium ions (3). Subunit 1 (Cox1) contains two heme *a* cofactors, one of which interacts with a mononuclear copper site (designated Cu_B) forming a heterobimetallic active site (heme a_3-Cu_B), whereas subunit 2 (Cox2) contains two copper ions in a binuclear center (designated Cu_A) (1).

Over 30 accessory proteins are necessary for the proper assembly of the enzyme (4, 5). The functional role of these accessory factors in the assembly of CcO concerns the formation and insertion of heme *a*, the delivery and insertion of metal ions to corresponding binding sites, and the final maturation of this multi-subunit enzyme. Six proteins (Cox11, Cox17, Cox19, Cox23, Sco2, and Sco1) have been identified to be implicated in the delivery and insertion of copper ions into CcO (3).

Cox17 is the copper metallochaperone within the IMS acting as the donor of Cu(I) to both Sco1 and Cox11 (6). Cox17, which contains six conserved cysteines, can in principle exist in the IMS in three different oxidation states: from the fully oxidized protein with three disulfide bonds to a partially oxidized form with two disulfide bonds or to a fully reduced state where no disulfide bonds are present (7, 8). These forms vary in terms of structural features and of metal binding ability. The partially oxidized state can bind one Cu(I) ion ($Cu_1(I)Cox17_{2S\text{-}S}$ hereafter), whereas the fully oxidized state is not able to bind copper (7). The structure of Cox17 from *Saccharomyces cerevisiae* was recently determined (9, 10). From this characterization it results that Cox17 has a structural organization with an α-helical hairpin domain preceded by an unstructured N-terminal segment (9). The fully reduced form is on the contrary present in a molten globule state where the six free cysteines cooperatively bind four Cu(I) ions forming a tetracopper-thiolate cluster ($Cu(I)_4Cox17$ hereafter) (7, 9, 11).

* This work was supported by European Commission: European Network of Research Infrastructures for Providing Access and Technological Advancements in bio-NMR Contract 026145, SPINE II Contract LSHG-CT-2006-031220 "From Receptor to Gene: Structures of Complexes from Signalling Pathways Linking Immunology, Neurobiology and Cancer," and Marie Curie Host Fellowship for Early Stage Research Training MEST-CT-2004-504391 "NMR in Inorganic Structural Biology." This work was also supported in part by the Italian MURST COFIN03 and MIUR-FIRB (Fondo per gli Investimenti della Ricerca di Base, Grant protocollo MIUR-RBLA032ZM7) and by Estonian Science Foundation Project 7191. The costs of publication of this article were defrayed in part by the payment of page charges. This article must therefore be hereby marked "*advertisement*" in accordance with 18 U.S.C. Section 1734 solely to indicate this fact.

The atomic coordinates and structure factors (codes 2RN9 and 2RNB) have been deposited in the Protein Data Bank, Research Collaboratory for Structural Bioinformatics, Rutgers University, New Brunswick, NJ (http://www.rcsb.org/).

[S] The on-line version of this article (available at http://www.jbc.org) contains supplemental Tables S1–S6 and Figs. S1–S3.

[1] To whom correspondence should be addressed: CERM and Dept. of Chemistry, University of Florence, Via L. Sacconi 6, Sesto Fiorentino, Italy 50019. Tel.: 39-055-4574272; Fax: 39-055-4574271; E-mail: ivanobertini@cerm.unifi.it.

[2] The abbreviations used are: CcO, cytochrome *c* oxidase; IMS, intermembrane space; GST, glutathione *S*-transferase; ESI, electrospray ionization; MS, mass spectrometry; DTT, dithiothreitol; HPLC, high pressure liquid chromatography; Q-TOF, quantitative time-of-flight; NOE, nuclear Overhauser effect; NOESY, NOE spectroscopy; HSQC, heteronuclear single quantum correlation.

Recently, it has been found in yeast that Cox17 import into the IMS is catalyzed by a disulfide relay system involving Mia40 and Erv1 proteins, which favor the formation of the partially oxidized $Cox17_{2S\text{-}S}$ state (12). It has been also found *in vitro* that $Cu(I)_1Cox17_{2S\text{-}S}$ and not $Cu(I)_4Cox17$ transfers Cu(I) to apoWT-HSco1 (13). These data suggest that the $Cox17_{2S\text{-}S}$ form is the active state in the copper transfer within the IMS.

In this paper we report the structural characterization of human Cox17 in the partially ($HCox17_{2S\text{-}S}$ hereafter) and fully oxidized ($HCox17_{3S\text{-}S}$ hereafter) states. The effect of reducing agents on $HCox17_{3S\text{-}S}$ was also investigated. Finally, the structure and backbone dynamics of $Cu(I)_1HCox17_{2S\text{-}S}$ are reported and compared with those of $apoHCox17_{2S\text{-}S}$. Two consecutive cysteines binds copper(I) ion, and this is the first example of a Cys-Cys binding motif in copper proteins. Until now, the structure of the partially oxidized form (*i.e.* with two disulfides) is available only for the demetallated form of the yeast homologue (9).

EXPERIMENTAL PROCEDURES

Protein Production and Copper Binding—The *hcox17* gene was amplified by PCR from a pET-11c expression vector already containing the human Cox17 cDNA (8). The *hcox17* gene was cloned into the Gateway Entry vector pENTR/tobacco etch virus/D-topoisomerase (Invitrogen), and subcloned into pETG-30A (European Molecular Biology Laboratory Protein Expression and Purification Facility) by Gateway LR reaction to generate an N-terminal, His-GST fused protein. The protein is expressed in *Escherichia coli* BL21-Origami(DE3) cells (Stratagene), which were grown in Luria-Bertani and minimal medium ($(^{15}NH_4)_2SO_4$ and/or [^{13}C]glucose) for the production of labeled samples. Protein expression was induced with 0.7 mM isopropyl β-D-thiogalactopyranoside for 16 h at 298 K. Purification was performed by using a HiTrap chelating HP column (Amersham Biosciences) charged with Zn(II) ions. His-GST tag was cleaved with AcTEV proteases. The digested protein was concentrated by ultrafiltration and loaded in a 16/60 Superdex 75 chromatographic column (Amersham Biosciences) to separate HCox17 from the N-terminal His-GST domain. The fractions showing a single component by SDS/PAGE were collected, and the protein concentration was measured using the Bradford protein assay (14). The pure protein was obtained in the apo form as checked by inductively coupled plasma MS and ESI-MS. HCox17 protein expressed following the above mentioned procedure contains four additional amino acids (GSFT), corresponding to the TEV protease recognition site, at the N terminus. Recombinant native human Cox17, where the first Met is processed away posttranslationally, was used for ESI MS/MS analysis and was produced as already described (8). The numbering of both HCox17 constructs follows the isolated, functional mammalian Cox17 sequences (15, 16) where the first Met is processed away posttranslationally. Therefore, the HCox17 sequence numbering starts proline 1.

The reduction of disulfide formed by the two consecutive cysteines, Cys^{22} and Cys^{23}, is almost instantaneous upon addition of 1 mM DTT under nitrogen atmosphere. The $apoHCox17_{2S\text{-}S}$ protein was then exchanged under anaerobic conditions into 50 mM phosphate, 1 mM DTT buffer at pH 7.2 using a PD-10 desalting column (Amersham Biosciences) and then concentrated by ultrafiltration to produce the final NMR sample. The Cu(I) form was obtained under anaeroboic conditions by addition of a slight excess of $(Cu(I)(CH_3CN)_4)PF_6$ directly to the final NMR $apoHCox17_{2S\text{-}S}$ sample (0.5–1 mM). Copper excess was then removed dialyzing the sample against NMR buffer or through PD-10 desalting column. The NMR sample of the $HCox17_{3S\text{-}S}$ form was obtained by air oxidation in about 2 days after the removal of 1 mM DTT, through PD-10 desalting column, from the final $apoHCox17_{2S\text{-}S}$ sample.

Far-UV CD spectra (190–260 nm) on the various forms of HCox17 were recorded on JASCO J-810 spectropolarimeter. Each spectrum was obtained as the average of four scans and corrected by subtracting the contributions from the buffer. A 0.6 mM $apoHCox17_{2S\text{-}S}$ sample was divided in different fraction and each one was incubated for 1 h under anaerobic atmosphere with different DTT concentrations (0, 15, and 20 mM). Each sample was then diluted in 10 mM phosphate buffer, pH 7.2, to obtain a 15–30 μM final protein concentration, and CD spectra were recorded. All of the steps were performed under nitrogen atmosphere using a degassed buffer. Quantitative estimate of the secondary structure contents was made by using the DICROPROT software package (17).

ESI MS/MS Analysis of Disulfide Pattern in HCox17—Recombinant human $Cox17_{3S\text{-}S}$ (35 μM) was reduced with 1 mM DTT in 20 mM ammonium acetate buffer, pH 7.5, for 1 min at 25 °C, and the resultant $Cox17_{2S\text{-}S}$ was alkylated with 5 mM iodoacetamide (1 h at 25 °C in dark). Carboxamidomethylated $Cox17_{2S\text{-}S}$ was desalted using HiTRAP™ desalting column (5 ml) (Amersham Biosciences) into 20 mM ammonium acetate buffer, pH 7.5, and two stable disulfides were reduced with 2 mM DTT at 55 °C (incubation time, 120 min). Resultant $Cox17_{0S\text{-}S}$ with two covalently attached carboxamidomethyl groups was digested with trypsin (using ratio 1:20) at 37 °C for 30 min. The reaction products were separated on a reverse phase HPLC column Agilent Eclipse XDB-C18 (4.6 × 150 mm; bead size, 5 μm) by using a gradient from 5–40% of buffer B over 5 column volumes. Buffer A was 0.1% trifluoroacetic acid in water, and buffer B was 0.1% trifluoroacetic acid in 95% acetonitrile. The fraction containing Cox17 peptide of 1530.73 Da (KPLKPCCACPETK, residues 17–29 with two covalently attached carboxamidomethyl groups) was injected at 5 μl/min into ESI-Q-TOF MS/MS instrument QSTAR Elite from Applied Biosystems (Foster City, CA) and analyzed in TOF MS and Q-TOF MS/MS mode. In MS/MS experiment a doubly protonated peak at 766.38 Da was selected for fragmentation, and collision energy between 40 and 60 CE was applied. Obtained MS/MS data were analyzed by program Bioanalyst 2.0 from Applied Biosystems. $Cu(I)_1HCox17_{2S\text{-}S}$ was produced by adding two equivalents of Cu(I)DTT complex to 40 μM $HCox17_{2S\text{-}S}$, which was obtained by reduction of $HCox17_{3S\text{-}S}$ as described above. Resultant $Cu(I)_1HCox17_{2S\text{-}S}$ was alkylated with 5 mM iodoacetamide after 120 min of incubation with copper ions. Carboxamidomethylated $Cox17_{2S\text{-}S}$ was desalted, reduced, and trypsinolyzed as described above. Reaction products were separated by reverse phase HPLC as described above, and fraction containing Cox17 peptide of 3178.49-Da (PGLVD-

SNPAPPESQEKKPLKPCCACPETK; residues 1–29 with two covalently attached carboxamidomethyl groups) was injected at 5 μl/min into ESI-Q-TOF MS/MS instrument QSTAR Elite from Applied Biosystems and analyzed in TOF MS and Q-TOF MS/MS mode. In MS/MS experiment a triply protonated peak at 1060.55 Da was selected for fragmentation, and collision energy between 40 and 60 CE was applied. Obtained MS/MS data were analyzed as described above.

NMR Spectroscopy—All of the NMR experiments used for resonance assignment and structure calculations were performed on 0.5–1 mM $^{13}C,^{15}N$ labeled $HCox17_{2S\text{-}S}$ and $HCox17_{3S\text{-}S}$ samples in 50 mM phosphate buffer, pH 7.2, containing 10% D_2O (plus 1 mM DTT for $HCox17_{2S\text{-}S}$) and are summarized in supplemental Table S1. All of the NMR spectra were collected at 298 K, processed using the standard Bruker software (XWINNMR), and analyzed through CARA program (18). The ^{1}H, ^{13}C, and ^{15}N resonance assignments of $apoHCox17_{2S\text{-}S}$, $Cu_1(I)HCox17_{2S\text{-}S}$, and $apoHCox17_{3S\text{-}S}$ are reported in supplemental Tables S2–S4. In particular, in both apo and $Cu(I)_1HCox17_{2S\text{-}S}$ forms, four cysteine residues, *i.e.* Cys^{25}, Cys^{35}, Cys^{44}, and Cys^{54}, have $C\beta$ chemical shift values typical of cysteines engaged in disulfide bonds ($C\beta^{25}$ = 40.6 (apo), 40.8 (Cu(I)), $C\beta^{35}$ = 36.6 (apo), 36.6 (Cu(I)), $C\beta^{44}$ = 39.5 (apo), 39.6 (Cu(I)), and $C\beta^{54}$ = 38.8 (apo), 39.0 (Cu(I)) ppm) (19). The two vicinal cysteines Cys^{22} and Cys^{23} are instead reduced ($C\beta^{22}$ = 28.7 (Cu(I)) and $C\beta^{23}$ = 25.7 (apo), 30.0 (Cu(I)) ppm). In $HCox17_{3S\text{-}S}$ form, all of the cysteines have $C\beta$ chemical shift values typical of cysteines engaged in disulfide bonds ($C\beta^{22}$ = 46.5, $C\beta^{23}$ = 46.0, $C\beta^{25}$ = 40.7, $C\beta^{35}$ = 36.6, $C\beta^{44}$ = 39.5, and $C\beta^{54}$ = 38.8 ppm).

Structure calculations were performed with the software package ATNOS/CANDID/CYANA (20–22), using as input the amino acid sequence, the chemical shift lists, and three $^{1}H,^{1}H$ NOE experiments: two-dimensional NOESY, three-dimensional ^{13}C-resolved NOESY, and three-dimensional ^{15}N-resolved NOESY recorded at 800 and 900 MHz with a mixing time of 100 ms. The standard protocol with seven cycles of peak picking using ATNOS, NOE assignment with CANDID, and structure calculation with CYANA-2.1 (22) was applied. ϕ and ψ dihedral angle constraints were derived from the chemical shift index (23) and TALOS analysis (24). In each ATNOS/CANDID cycle, the angle constraints were combined with the updated NOE upper distance constraints in the input for the subsequent CYANA-2.1 structure calculation cycle. In the seventh ATNOS/CANDID/CYANA cycle, a total of 2366 or 2203 NOE cross-peaks were assigned from 2825 or 2555 peaks picked in the spectra of $apoHCox17_{2S\text{-}S}$ and $Cu_1(I)HCox17_{2S\text{-}S}$, respectively, which yielded 939 or 834 meaningful NOE upper distance limits. In addition, two disulfide bonds between Cys^{35} and Cys^{44} and between Cys^{25} and Cys^{54} were imposed, as resulted from their ^{13}C chemical shift analysis, by adding two lower and two upper distance constraints of 2.0 and 2.1 Å, respectively, between the Sγ atoms. The copper(I) ion was finally included in the calculations of the copper-loaded form by adding a new residue in the amino acid sequence. This residue is formed from a chain of dummy atoms with zero van der Waals' radii, so that they can freely penetrate into the protein, and by one atom with a radius of 1.4 Å, which mimics the copper ion. The sulfur atoms of Cys ligands were linked to the metal ion through upper distance limits of 2.3 Å, according to the yeast Cox17 Sγ-Cu(I) distance (25). This approach does not impose any fixed orientation of the ligands with respect to the copper ion.

The 20 conformers with the lowest residual target function values were subjected to restrained energy minimization in explicit water with AMBER 8.0 (26). NOE and torsion angle constraints were applied with force constants of 50 kcal mol^{-1} $Å^{-2}$ and 32 kcal mol^{-1} rad^{-2}, respectively. The force field parameters for the copper(I) ion and the ligands were adapted from those already reported for similar copper(I) sites in copper proteins (27, 28). The quality of the structures was evaluated using the programs PROCHECK, PROCHECK-NMR (29), and WHATIF (30).

The root mean square deviation to the mean structure for the structured region of the protein (residues 24–61) is 0.32 ± 0.07 Å for the backbone and 0.74 ± 0.07 Å for all heavy atoms for $apoHCox17_{2S\text{-}S}$ and 0.31 ± 0.09 Å for the backbone and 0.72 ± 0.11 Å for all heavy atoms for $Cu_1(I)HCox17_{2S\text{-}S}$. The conformational and energetic analysis of both structures are reported in supplemental Tables S5 and S6.

The atomic coordinates, structural restraints, and resonance assignments of $apoHCox17_{2S\text{-}S}$ and $Cu_1(I)HCox17_{2S\text{-}S}$ have been deposited in the Protein Data Bank Resonance (PDB ID 2RN9 and 2RN8) and BioMagResBank (BRMB codes 11019 and 11020).

Relaxation experiments were performed on ^{15}N-labeled samples at 500 MHz. The ^{15}N backbone longitudinal (R_1) and transverse (R_2) relaxation rates as well as heteronuclear $^{15}N\{^{1}H\}$ NOEs were measured as previously described (31, 32). ^{15}N relaxation parameters were then analyzed following the standard Tensor2 protocol (33).

Disulfide reduction of $HCox17_{2S\text{-}S}$ and $HCox17_{3S\text{-}S}$ forms was followed by NMR. To a 1:1 mixture of apo and $Cu_1(I)HCox17_{2S\text{-}S}$ or to $HCox17_{3S\text{-}S}$, both in 50 mM phosphate buffer, pH 7.2, containing 10% D_2O, up to 20 mM or 1 mM DTT was added stepwise in anaerobic conditions, respectively, and two-dimensional ^{1}H-^{15}N HSQC spectra were acquired.

RESULTS

Human Cox17 in the fully oxidized and partially oxidized states, *i.e.* with three or two disulfide bonds, shows ^{1}H-^{15}N HSQC spectra with good signal spreading in both the apo and Cu(I) bound forms but also with a number of signals clustered in the central region of the spectrum, which is typical of unfolded polypeptides (amide proton resonances clustered between 8 and 8.5 ppm) (Fig. 1). This suggests that the protein contains both structured and unstructured regions. From the chemical shift index (23) and ^{3}J-coupling analysis, it appears indeed that all three protein forms have two helices (segments 26–38 and 45–57), whereas the rest of the protein is not in any secondary structure element. The NH signals clustered in the central region of ^{1}H-^{15}N HSQC spectra, which belong to the first 17 amino acids of the protein, experience negative $^{15}N\{^{1}H\}$ NOE values indicating that they are highly flexible (see below). The partially oxidized form of HCox17 has features similar to those of the yeast homologue (9).

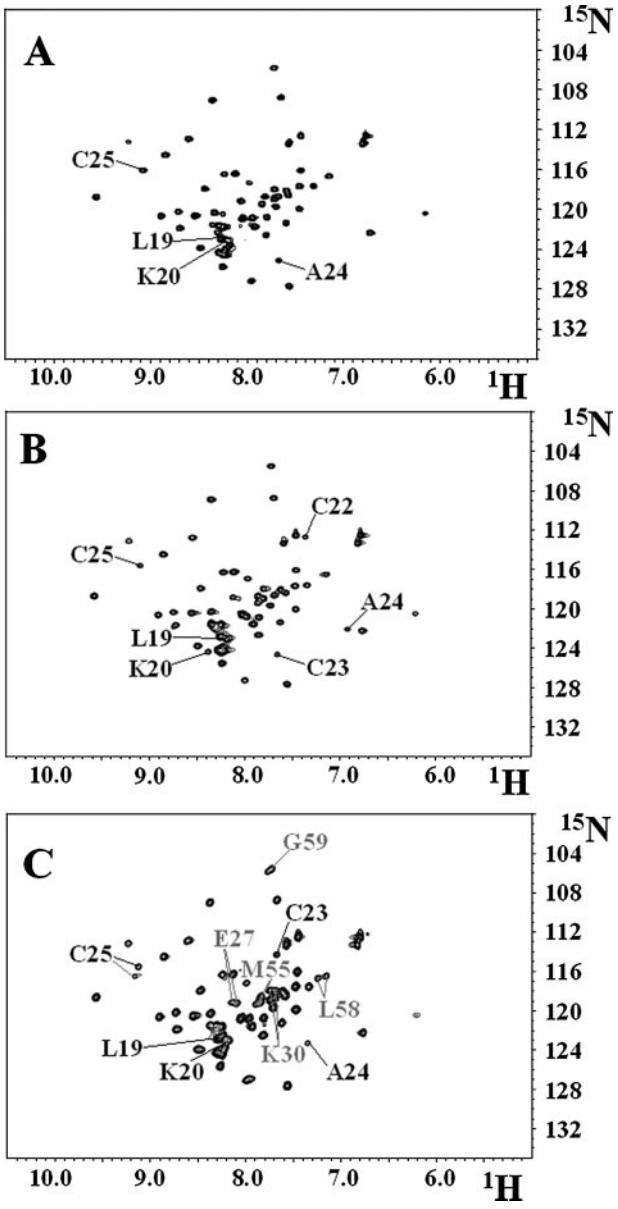

FIGURE 1. **^{1}H-^{15}N HSQC maps of apoHCox17$_{2S\text{-}S}$ (*A*), Cu$_1$(I)HCox17$_{2S\text{-}S}$ (*B*), and HCox17$_{3S\text{-}S}$ (*C*) at 298K and pH 7.2 in 50 mM phosphate buffer.** 1 mM DTT is present in the buffer of the apoHCox17$_{2S\text{-}S}$ and Cu$_1$(I)HCox17$_{2S\text{-}S}$ forms. Cross-peaks of the residues in the metal-binding region are indicated in *black*. Cross-peaks of the NHs showing two conformations in the HCox17$_{3S\text{-}S}$ protein are indicated in *gray*.

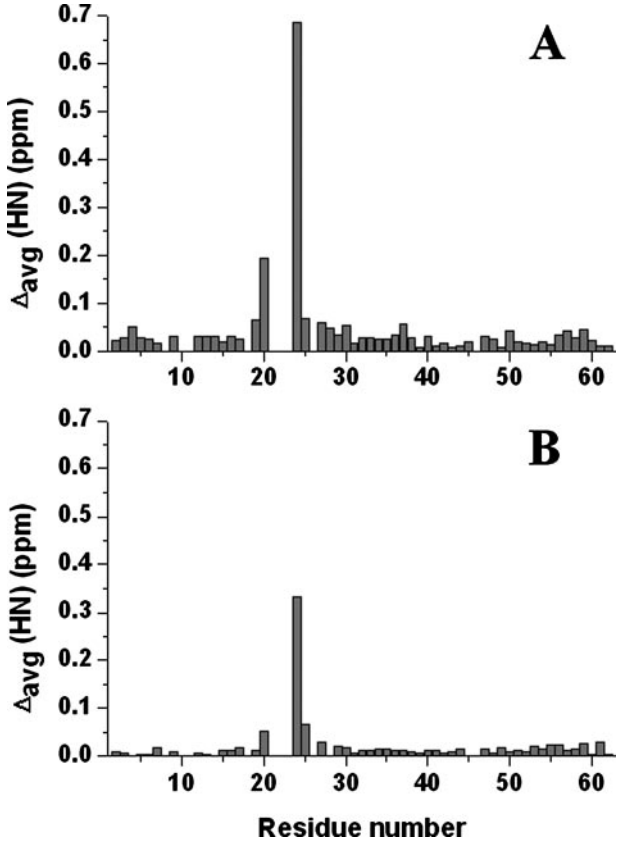

FIGURE 2. **The weighted average chemical shift differences (Δ_{avg}(*HN*)) between apoHCox17$_{2S\text{-}S}$ and Cu$_1$(I)HCox17$_{2S\text{-}S}$ (*A*) and between apoHCox17$_{2S\text{-}S}$ and HCox17$_{3S\text{-}S}$ (*B*).** $\Delta_{avg}(HN) = \{[(\Delta H)^2 + (\Delta N/5)^2]/2\}^{1/2}$, where ΔH and ΔN are chemical shift differences for ^{1}H and ^{15}N, respectively.

The ^{13}C resonances of all six cysteines have been assigned for the three Cox17 forms, with the exception of Cys^{22} in the apoHCox17$_{2S\text{-}S}$ state. In both apo and Cu(I)$_1$HCox17$_{2S\text{-}S}$, the chemical shifts of the Cβ atoms of Cys^{25}, Cys^{35}, Cys^{44}, and Cys^{54} are typical of cysteines engaged in disulfide bonds (19), whereas those of Cys^{22} and Cys^{23} in the Cu(I) form and of Cys^{23} in the apo form (Cys^{22} is not detected) are typical of cysteines in the reduced state. On the contrary, in the HCox17$_{3S\text{-}S}$ state, the chemical shifts of the Cβ atoms of all Cys indicate that all the cysteines are engaged in disulfide bonds.

Few NH signals of HCox17$_{2S\text{-}S}$ exhibit significant spectral variations upon Cu(I) addition (Fig. 2), the most dramatic ones being for residues 20–24, which comprise the metal binding motif Cys^{22}–Cys^{23}. These residues indeed experience, upon metal addition, either large chemical shift variations (Lys^{20} and Ala^{24}) (Fig. 2) or the appearance of their NH signals (Cys^{22} and Cys^{23}), which are not observed in the apo state (Fig. 1). A similar trend is observed going from the partially oxidized HCox17$_{2S\text{-}S}$ state toward fully oxidized HCox17$_{3S\text{-}S}$ one. Significant spectral changes are indeed observed only in the vicinity of the two Cys involved in the formation of the third disulfide bond, where either chemical shift variations (A24) (Fig. 2) or the appearance of the NH signal of Cys^{23} are occurring (Fig. 1). These data suggest that both copper(I) binding to HCox17$_{2S\text{-}S}$ as well as the formation of the third disulfide essentially determines local structural changes restricted to the Cys^{22}-Cys^{23}-Ala^{24} region. However, at variance with the HCox17$_{2S\text{-}S}$ state, in HCox17$_{3S\text{-}S}$ some NHs (Gly^{59}, Leu^{58}, Met^{55}, Lys^{30}, Glu^{27}, and Cys^{25}) located in the vicinity of the Cys^{22}-Cys^{23}-Ala^{24} motif display two conformations as detected in the ^{1}H-^{15}N HSQC map (Fig. 1), indicating that the disulfide bond formation determines a structural heterogeneity in the surrounding of this region. Double conformations have been reported to occur for disulfide bonds as a result of their isomerization (34).

The structures of apoHCox17$_{2S\text{-}S}$, Cu$_1$(I)HCox17$_{2S\text{-}S}$, and apoHCox17$_{3S\text{-}S}$ have the coiled coil-helix-coiled coil-helix structural motif (*CHCH*) (Fig. 3) as observed in the yeast homologue (9, 10). This structural motif is predicted to be common to several mitochondrial proteins like Cox19 (35) and Cox23 (36), which are, similar to Cox17, involved in copper ion insertion into CcO (3), Mia40, which is required for the import of Cox17

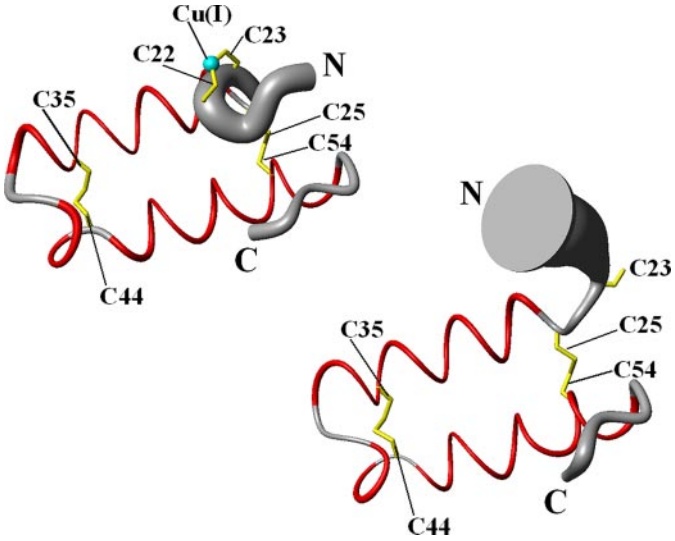

FIGURE 3. **Solution structures (residues 18–62) of Cu_1(I)$HCox17_{2S\text{-}S}$ (*top*) and $apoHCox17_{2S\text{-}S}$ (*bottom*) represented as a tube with a radius proportional to the backbone root mean square deviation of each residue.** The first 17 amino acids are completely unstructured in both forms and therefore are removed. The secondary structure elements, two α-helices (residues 26–38 and 45–57) and a 3_{10}-helix (residues 41–43), are in *red*. The copper(I) ion (*cyan*) and the Cys residues (*yellow*) involved in copper binding (Cys^{22} and Cys^{23}) and disulfide bridges (Cys^{25}, Cys^{35}, Cys^{44}, and Cys^{54}) are shown.

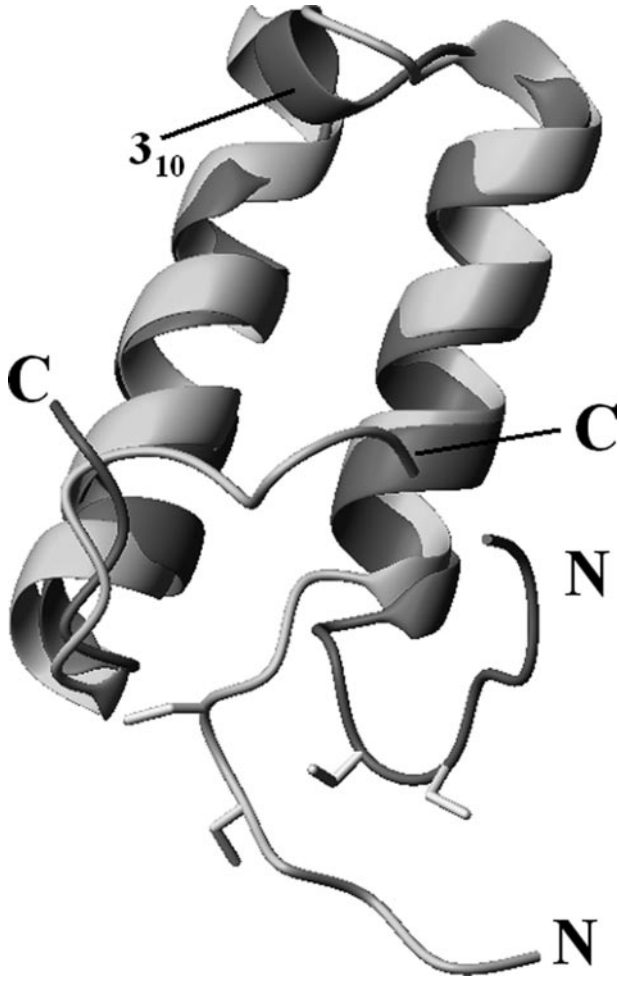

FIGURE 4. **Comparison of the backbone of human $apoCox17_{2S\text{-}S}$ (*gray*) and yeast $apoCox17_{2S\text{-}S}$ (*light gray*).** The amino acids at the N termini of both proteins have been removed because they are completely unstructured. The cysteine residues are indicated in *yellow*, and the 3_{10} helix present in both apo and $Cu(I)_1HCox17_{2S\text{-}S}$ solution structures is also indicated.

and Cox19 into the IMS (37), and to several other IMS proteins whose functions are unrelated to CcO assembly (38). Accordingly, all the above proteins have four cysteine residues organized in the twin CX_9C motif, located at the N- and C-terminal ends of each helix of the predicted *CHCH* motif. These conserved cysteines are those that form two interhelical disulfide bonds (Fig. 3), thus forcing the two helices to get close each other in an antiparallel mode forming an α-hairpin. The global backbone root mean square deviation value (calculated on the structured region) between yeast and human $Cox17_{2S\text{-}S}$ structures is low (1.4 Å). The only meaningful structural difference between them is found at the N-terminal part of the second helix, which is indeed shorter in $HCox17_{2S\text{-}S}$ of one turn but, at variance with yeast $Cox17_{2S\text{-}S}$, is followed by a 3_{10} helix (Fig. 4).

Copper(I) ion in Cu_1(I)$HCox17_{2S\text{-}S}$ is coordinated by the sulfurs of two adjacent Cys, forming a S-Cu-S angle of about 130° (Fig. 3). The two copper-binding cysteines, which are conserved in all Cox17 proteins, are the ones adjacent within the Cys^{22}-Cys^{23}-Ala^{24}-Cys^{25} motif. No other protein atoms appear close enough (<2.5 Å) to be the third copper(I) ligand in $HCox17_{2S\text{-}S}$. From the structure and the ^{2}J NH coupling-based ^{1}H-^{15}N HSQC experiment, it results that all the three His, potential ligands of copper, are protonated on Nϵ2, and no one is coordinated to the metal ion (39, 40). The coordination sphere of Cu(I), which is extensively solvent exposed, could be completed by an exogenous molecule, such as DTT, which is present in the sample in 1 mM concentration. Such tricoordinated sulfur environment has been already suggested in several members (Atx1, Hah1, and CopZ) of a cytoplasmic metallochaperone family (41–43).

$Cu(I)_1HCox17_{2S\text{-}S}$ and $apoHCox17_{2S\text{-}S}$ were also studied by ESI MS/MS analysis to characterize the metal-binding cysteines. For this purpose both $Cu_1HCox17_{2S\text{-}S}$ and $apoHCox17_{2S\text{-}S}$ were treated with iodoacetamide, which is able to alkylate reduced cysteine, and these modified residues were identified by MS/MS analysis of trypsinolytic peptides containing CCAC fragment. Analysis of doubly carboxamidomethylated peptide fragment 17–29 (KPLKPCCACPETK), obtained from $apoHCox17_{2S\text{-}S}$, indicated that the first two adjacent Cys residues (Cys^{22} and Cys^{23}) were carboxamidomethylated, whereas Cys^{25} of the peptide was unmodified (supplemental Fig. S1). After alkylation and trypsinolytic treatment of $Cu(I)_1HCox17_{2S\text{-}S}$, we identified by ESI-MS peptide 1–29 (PGLVDSNPAPPESQEKKPLKPCCACPETK) where two of the three contained Cys are covalently attached by carboxamidomethyl groups (3178.49 Da). Theoretical molecular mass of peptide 1–29 is 3064.54 Da, whereas theoretical molecular mass of peptide 1–29 with two carboxamidomethylated Cys residues is 3178.54 Da. From MS/MS spectra of peptide 1–29 we identified following masses: 473.25, 576.26, and 647.29 Da, which correspond to y_4 (PETK), y_5 (C^{25}PETK), y_6 (AC^{25}PETK) fragment, and 807.30 Da, which corresponds to fragment y_7 ($C^{23}AC^{25}$PETK) containing one carboxamidomethylated Cys residue. Overall, these results indicate that the two adjacent Cys residues (Cys^{22} and Cys^{23}) are both carboxamidomethylated, whereas the remaining Cys^{25} of the peptide is not alkylated.

Thus, in both apo and $Cu(I)_1HCox17_{2S\text{-}S}$, the two adjacent Cys residues (Cys^{22} and Cys^{23}) are in reduced state, in agreement with NMR results.

The heteronuclear relaxation data on both $apoHCox17_{2S\text{-}S}$ and $Cu_1(I)HCox17_{2S\text{-}S}$ (supplemental Fig. S2) point at two protein regions with distinct motional regimes, one for the first 17 amino acids and the other for the 25–62 segment of the protein. The N-terminal region is characterized by negative $^{15}N\{^1H\}$ NOE values that indicate the presence of motions faster than the overall molecular tumbling. Also, the S^2 values, estimated through a model-free approach with Tensor2 program (33), are quite low for the N-terminal segment (residues 2–17), being 0.40 ± 0.09 in the apo form and 0.36 ± 0.16 in the Cu(I) form. On the contrary, the majority of residues in the 25–62 segment are more rigid in both forms (supplemental Fig. S2). However, the 25–62 segment of $apoHCox17_{2S\text{-}S}$ shows fast backbone NH motions with larger amplitude than $Cu_1(I)HCox17_{2S\text{-}S}$, as resulted from its lower average S^2 parameter (S^2 (apo) = 0.65 ± 0.14 *versus* S^2 (Cu(I)) = 0.86 ± 0.13). At variance with $Cu_1(I)HCox17_{2S\text{-}S}$, backbone NH motions of several residues belonging to the 25–62 segment of $apoHCox17_{2S\text{-}S}$ are also characterized by exchange contributions (R_{ex}) to their relaxation. Backbone NHs of the five, non-proline, residues in between the unstructured N-terminal tail and the 25–62 segment, comprising the CCAC motif display conformational motions much more pronounced in $apoHCox17_{2S\text{-}S}$ than in $Cu(I)_1HCox17_{2S\text{-}S}$. NHs of the copper(I)-binding cysteines are indeed not detected in the apo form, likely as a consequence of exchange processes, whereas their NH cross-peaks appear upon copper(I) binding, indicating a more rigid backbone conformation in the latter form. However, their R_2 values in $Cu(I)_1HCox17_{2S\text{-}S}$ are higher than the average (calculated on the 25–61 segment) (supplemental Fig. S2), indicating that a certain degree of conformational mobility is still present. Copper(I) binding also reduces the backbone flexibility of Leu^{19} and Lys^{20}. Their $^{15}N\{^1H\}$ NOE negative in the apo form indicate motions faster than the overall molecular tumbling rate, whereas positive values in the copper(I) form indicate a decreased flexibility (supplemental Fig. S2). In conclusion, copper(I) binding drastically reduces the backbone motions in the metal-binding region of $HCox17_{2S\text{-}S}$.

Investigating the effect of reducing agents on $HCox17_{3S\text{-}S}$, $^1H\text{-}^{15}N$ HSQC data show that 1 mM DTT is able to easily reduce the disulfide bond formed within the CC motif in $Cox17_{3S\text{-}S}$, thus producing the partially oxidized $Cox17_{2S\text{-}S}$ form. NMR titration of a 1:1 mixture of apo and $Cu_1(I)HCox17_{2S\text{-}S}$ shows that the addition of 15 mM DTT is necessary to completely remove copper(I) ion, whereas the two disulfides within the *CHCH* motif can be reduced only with further additions of DTT up to 20 mM. At the latter DTT concentration, all of the signals that are spread out in the folded region of the $^1H\text{-}^{15}N$ spectrum of $apoHCox17_{2S\text{-}S}$ disappear, with the concomitant formation of new cross-peaks clustered in the spectral region typical of unstructured polypeptides (amide proton resonances between 8 and 8.5 ppm) (Fig. 5). The complete reduction of all disulfides of HCox17 therefore determines the formation of a state without a well defined tertiary structure. CD spectra of $apoHCox17_{2S\text{-}S}$ were then measured in the presence of various concentrations of DTT (supplemental Fig. S3) to address secondary structural variations occurring from the partially oxidized to the fully reduced states. At 1 mM DTT, $Cox17_{2S\text{-}S}$ exhibits the characteristic bands of α helix conformation, with double minima at 222 and 206 nm as well as a positive maximum at 192 nm. The fitting of the CD spectrum indicates an α-helical content of 40%. After overnight incubation with 20 mM DTT, thus obtaining the fully reduced species, the α-helical content is still about 30%. This indicates that the polypeptide chain has a high propensity to adopt a helical conformation even in a completely reduced state. This behavior together with that observed through NMR indicates therefore that the fully reduced form is essentially in a molten globule state and is the same observed in the yeast Cox17 homologue (9).

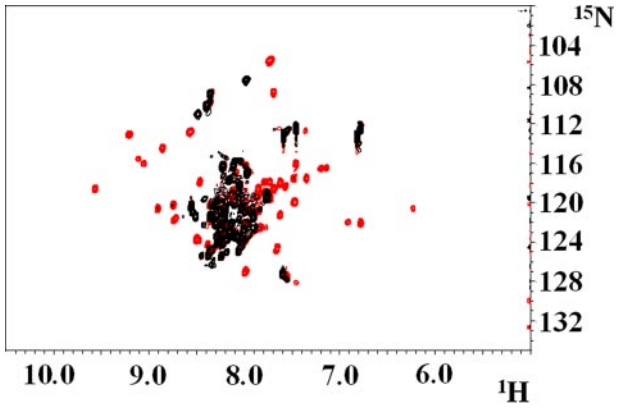

FIGURE 5. **Overlay of two-dimensional $^1H\text{-}^{15}N$ HSQC spectra of a 1:1 mixture of $Cu_1(I)HCox17_{2S\text{-}S}$ and $apoHCox17_{2S\text{-}S}$ in 1 mM DTT (*red contours*) and in 20 mM DTT (*black contours*).**

DISCUSSION

Human Cox17 in both apo and copper(I) forms is a protein constituted by a *CHCH* motif of about 40 residues plus an unstructured, flexible N-terminal tail of about 15 residues. The structural and dynamical properties of the residues in between these two regions (residues 17–24), which comprise the metal binding motif, are the only ones significantly modulated by the binding of copper(I) ion. The latter region in $apoHCox17_{2S\text{-}S}$ is indeed highly unstructured with a large degree of backbone flexibility, whereas upon copper(I) binding, it becomes more structured and less flexible. In particular, copper(I) binding determines local structural rearrangements around the two coordinating cysteines of the CC motif, determining the formation of a turn that positions the two consecutive Cys ligands close to each other in an optimal conformation for metal binding (Fig. 3). To our knowledge, this is the first example of a copper(I) ion coordinated by two consecutive Cys residues. Around the metal-binding region of $Cu(I)_1HCox17_{2S\text{-}S}$, no other protein atom is at bond distance, but in the second coordination sphere (<6.0 Å), the copper(I) ion is surrounded by two conserved charged residues, Lys^{20} and Lys^{29} (Fig. 6). In particular, Lys^{20}, located at the end of the CC turn above the metal ion, takes a well defined conformation very close to the copper(I) ion (mean distance in the family of conformers 4.5 Å); on the contrary, it is highly conformationally disordered in the copper-free form. The fast internal motions of Lys^{20} are also

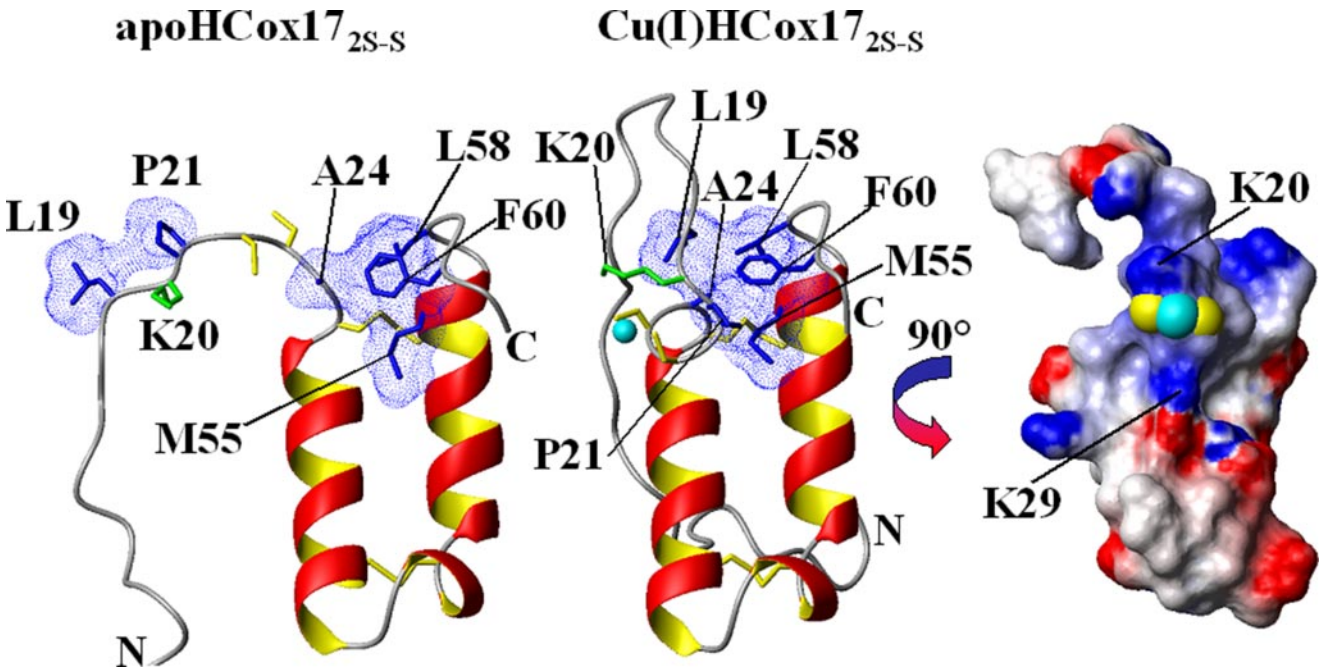

FIGURE 6. **Comparison of the solution structures of apo and Cu(I)$_1$HCox17$_{2S\text{-}S}$.** Side chain packing involving the hydrophobic residues (Leu[19], Pro[21], Ala[24], Met[55], Leu[58], and Phe[60]) in the metal binding surroundings is shown in *blue*. The cysteines residues are shown in *yellow*, Lys[20] is in green, and the copper(I) ion is in *cyan*. A rotated view of the electrostatic surface of Cu(I)$_1$HCox17$_{2S\text{-}S}$ is also shown on the *right*. The positively charged, negatively charged, and neutral amino acids are represented in *blue*, *red*, and *white*, respectively. The Cys[22] and Cys[23] sulfurs and the Cu(I) ion are shown as *yellow* and *cyan spheres*, respectively.

highly reduced upon copper(I) binding. These features strongly resemble those of the copper-binding region of a well characterized cytosolic metallochaperone, Atx1 (44). It has been found that the eukaryotic chaperones possess a conserved lysine residue located adjacent to the copper-binding site (27). This lysine (Lys[65] in yeast Atx1) has been proposed to have a functional role in stabilizing copper binding (27) and modulating copper transfer (45). Therefore, we suggest that, similarly to yeast Atx1, the proximity of Lys[20], which takes a defined conformation in the copper form, contributes to the stabilization of the overall negative charge resulting from binding of Cu(I) to two cysteinate anions. Its approach toward the copper site could represent a local rearrangement of the protein structure for optimizing the electrostatic interactions upon copper binding. The effect of a mutation on this position is also similar in the two proteins, because its change to an Ala residue leaves a still functional protein in both cases (46, 47), suggesting that a neutral residue at this position appears well tolerated in both cases. Negative charge is, however, not well tolerated in this position, resulting indeed in a compromised function for the Atx1 chaperone (47).

Another important structural feature of the metal binding surroundings, helping to organize the copper ligands and Lys[20] in the appropriate orientation for metal binding, is determined by the hydrophobic contacts between the residues located at the end of the C-terminal helix (Met[55], Leu[58], and Phe[60]) with those at the N terminus (Leu[19], Pro[21], and Ala[24]) (Fig. 6). All of these residues, which are highly conserved in homologous sequences, form in Cu(I)$_1$HCox17$_{2S\text{-}S}$ a compact hydrophobic patch that orients the cysteine thiols, and Lys[20], toward the protein surface and exposed to the solvent (Fig. 6), thus favoring an efficient metal transfer with the protein partners, according

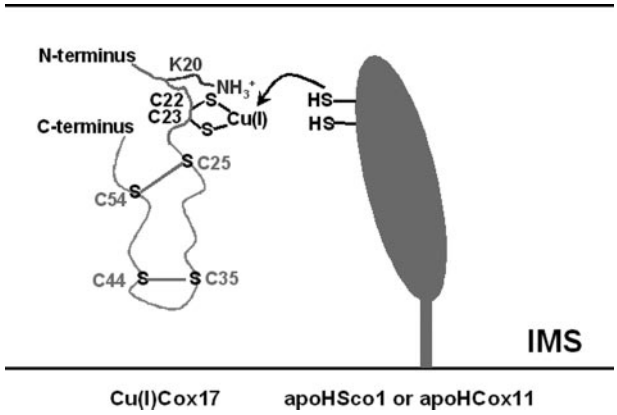

FIGURE 7. **Copper transfer from Cu(I)$_1$HCox17$_{2S\text{-}S}$ to its protein partners, apoHSco1 and apoHCox11, occurring in the IMS is depicted.** The solvent exposed metal-binding site of HCox17$_{2S\text{-}S}$ can easily be accessible for coordination by a further thiol group of a cysteine residue belonging to apoHSco1 or apoHCox11. Cys residues involved in the two disulfide bonds within *CHCH* motif are not involved in the metal transfer mechanism as a consequence of their high stability toward reduction.

to the metallochaperone function of this protein in the IMS (Fig. 7). In the apoHCox17$_{2S\text{-}S}$ form this hydrophobic patch is partially destabilized by the higher degree of backbone flexibility of the residues at the N terminus, determining less compact hydrophobic interactions (Fig. 6). This behavior is again similar to what was observed for the Atx1 metallochaperone where, in the metal-binding region, less compact hydrophobic interactions associated with an increase of backbone motions are observed upon copper(I) release, determining a reduction of the first turn at the N terminus of helix α1 in the metal-binding site (27). Overall, from the analysis of the structural and dynamical properties, we can therefore conclude that the copper(I) form of Cox17$_{2S\text{-}S}$ has features specific to copper chaperones.

Concerning biological context, as human Cox17 displays several structural and dynamical properties that are typical of the cytoplasmic metallochaperone Atx1, it can therefore play a role within IMS for tightly controlling the copper concentration, similar to what it has been found in the cytoplasm where several systems of cellular copper transport, involving also Atx1, have been discovered (48). However, at variance with Atx1, the global fold of HCox17 is quite atypical with, indeed, a large unstructured segment. It is also completely unrelated to its protein partners Sco1 (49) and Cox11 (50), which in turn have different folds one from the other. Atx1 has, on the contrary, the same fold as its protein partner Ccc2a without the presence of unstructured regions (27, 51). These structural differences of the Cox17/Sco1/Cox11 pattern *versus* the Atx1/Ccc2a pattern can play an important role in modulating the metal transfer processes in different ways. Similar folds in the protein partners can be indeed important in determining a reversible copper transfer mechanism, as found in the Atx1/Ccc2a interaction (52), whereas the different fold of the protein partners found in the Cox17/Sco1/Cox11 interactions can somehow have a role in the quantitative copper transfer observed for the Cox17/Sco1 pair (13), as well as in the recognition and binding to several different partners. In the case of the Cox17/Sco1 pairs, the quantitative copper transfer can be also driven by the higher number of Sco1 metal-binding ligands, with the copper(I) ion in Sco1 being indeed coordinated by two cysteines and one histidine far away in the sequence (49). The fold of HCox17 contains two CX_9C motifs and is typical of systems involved in Cys redox reaction within the IMS (38). In particular, the protein partner Mia40 (37) also has the twin CX_9C motifs, thus presumably having a similar fold that can be involved in the protein-protein recognition process occurring during HCox17 entrapment into the IMS. On the contrary, the K*X*CC motif is consistent with a chaperone function.

Human $Cox17_{3S\text{-}S}$ protein has an easily reducible disulfide bond, corresponding to the one involved in copper(I) binding, and two disulfides in the *CHCH* motif that are, on the contrary, highly stable toward reduction. These results support a model where, once the protein is maturated into the IMS forming the $Cox17_{2S\text{-}S}$ state through Mia40 assistance (12), it performs its function of copper(I) chaperone remaining in the latter redox state (Fig. 7), which can be thus considered the predominant one within the IMS, where the redox environment is likely more oxidative as compared with the cytosol (11, 53). On the contrary, the rupture of the two disulfide bonds within the CX_9C motifs in high reducing conditions (20 mM DTT), which reasonably mimic the cytosolic redox environment, determines the disruption of the α hairpin structure, generating a fully Cys-reduced molten globule state of HCox17 necessary for its import from the cytoplasm into the IMS (12).

It should be pointed out that replacement of the conserved Cys^{57} with a Ser does not perturb Cox17 function in yeast, at variance with the substitution of Cys^{26} with a Ser (54). Because the latter two cysteines are disulfide partners in the $HCox17_{2S\text{-}S}$ structure and are not involved in copper binding, it is possible that these mutations affect the protein import and/or retention mechanism into IMS via Mia40 (12, 55), preventing the formation of a functional Cox17 state only when Cys^{26} is mutated. Accordingly, their amount within the IMS is largely reduced with respect to that of wild-type protein (54). On the contrary, mutations of the other two disulfide-linked Cys in $HCox17_{2S\text{-}S}$ structure results in a functional protein in yeast (54), suggesting that they are not essentially perturbing Cox17 import. Cys^{22} and Cys^{23} are essential for CcO activity of yeast (54) because they are involved in $Cu(I)_1HCox17_{2S\text{-}S}$ structure in copper(I) binding, thus abolishing copper chaperone function. From this structural-functional analysis, we can suggest that the copper chaperone function of HCox17 relies essentially only in the availability of the K*X*CC motif, whereas the *CHCH* motif is important to allow HCox17 to be trapped in the IMS through the interaction with Mia40.

In conclusion, in this work we have elucidated the structural, dynamical, and redox properties of human apo and $Cu(I)Cox17_{2S\text{-}S}$ and discussed them in relation to their involvement in copper(I) transfer toward cytochrome *c* oxidase copper sites as well as in the protein import into the IMS.

Acknowledgments—We thank Anastassia Voronova and Nina Sokolova for technical assistance in protein expression and ESI MS experiments.

REFERENCES

1. Tsukihara, T., Aoyama, H., Yamashita, E., Tomizaki, T., Yamaguchi, H., Shinzawa-Itoh, K., Nakashima, R., Yaono, R., and Yoshikawa, S. (1995) *Science* **269,** 1069–1074
2. Beinert, H. (1995) *Chem. Biol.* **2,** 781–785
3. Carr, H. S., and Winge, D. R. (2003) *Acc. Chem. Res.* **36,** 309–316
4. Tzagoloff, A., and Dieckmann, C. L. (1990) *Microbiol. Rev.* **54,** 211–225
5. Barrientos, A., Barros, M. H., Valnot, I., Rotig, A., Rustin, P., and Tzagoloff, A. (2002) *Gene* (*Amst.*) **286,** 53–63
6. Horng, Y. C., Cobine, P. A., Maxfield, A. B., Carr, H. S., and Winge, D. R. (2004) *J. Biol. Chem.* **279,** 35334–35340
7. Palumaa, P., Kangur, L., Voronova, A., and Sillard, R. (2004) *Biochem. J.* **382,** 307–314
8. Voronova, A., Kazantseva, J., Tuuling, M., Sokolova, N., Sillard, R., and Palumaa, P. (2007) *Protein Expression Purif.* **53,** 138–144
9. Arnesano, F., Balatri, E., Banci, L., Bertini, I., and Winge, D. R. (2005) *Structure* **13,** 713–722
10. Abajian, C., Yatsunyk, L. A., Ramirez, B. E., and Rosenzweig, A. C. (2004) *J. Biol. Chem.* **279,** 53584–53592
11. Voronova, A., Meyer-Klaucke, W., Meyer, T., Rompel, A., Krebs, B., Kazantseva, J., Sillard, R., and Palumaa, P. (2007) *Biochem. J.* **408,** 139–148
12. Mesecke, N., Terziyska, N., Kozany, C., Baumann, F., Neupert, W., Hell, K., and Herrmann, J. M. (2005) *Cell* **121,** 1059–1069
13. Banci, L., Bertini, I., Ciofi-Baffoni, S., Leontari, I., Martinelli, M., Palumaa, P., Sillard, R., and Wang, S. (2007) *Proc. Natl. Acad. Sci. U. S. A.* **104,** 15–20
14. Bradford, M. (1976) *Anal. Biochem.* **72,** 248–254
15. Chen, Z. W., Bergman, T., Ostenson, C. G., Efendic, S., Mutt, V., and Jornvall, H. (1997) *Eur. J. Biochem.* **249,** 518–522
16. Takenouchi, T., Fujimoto, M., Shimamoto, A., and Munekata, E. (1999) *Biochim. Biophys. Acta* **1472,** 498–508
17. Deleage, G., and Geourjon, C. (1993) *Comp. Appl. Biosc.* **9,** 197–199
18. Keller, R. (2004) *The Computer Aided Resonance Assignment Tutorial*, CANTINA Verlag, Goldau
19. Sharma, D., and Rajarathnam, K. (2000) *J. Biomol. NMR* **18,** 165–171
20. Herrmann, T., Güntert, P., and Wüthrich, K. (2002) *J. Mol. Biol.* **319,** 209–227
21. Herrmann, T., Güntert, P., and Wüthrich, K. (2002) *J. Biomol. NMR* **24,** 171–189
22. Guntert, P. (2004) *Methods Mol. Biol.* **278,** 353–378

23. Wishart, D. S., and Sykes, B. D. (1994) *J. Biomol. NMR* **4,** 171–180
24. Cornilescu, G., Delaglio, F., and Bax, A. (1999) *J. Biomol. NMR* **13,** 289–302
25. Srinivasan, C., Posewitz, M. C., George, G. N., and Winge, D. R. (1998) *Biochemistry* **37,** 7572–7577
26. Case, D. A., Darden, T. A., Cheatham, T. E., Simmerling, C. L., Wang, J., Duke, R. E., Luo, R., Mertz, K. M., Wang, B., Pearlman, D. A., Crowley, M., Brozell, S., Tsui, V., Gohlke, H., Mongan, J., Hornak, V., Cui, G., Beroza, P., Schafmeister, C., Caldwell, J. W., Ross, W. S., and Kollman, P. A. (2004) AMBER 8, Version 8, University of California, San Francisco, CA
27. Arnesano, F., Banci, L., Bertini, I., Huffman, D. L., and O'Halloran, T. V. (2001) *Biochemistry* **40,** 1528–1539
28. Poger, D., Fuchs, H. J. R., Nedev, H., Ferrand, M., and Crouzy, S. (2005) *FEBS Lett.* **579,** 5287–5292
29. Laskowski, R. A., Rullmann, J. A. C., MacArthur, M. W., Kaptein, R., and Thornton, J. M. (1996) *J. Biomol. NMR* **8,** 477–486
30. Vriend, G. (1990) *J. Mol. Graphics* **8,** 52–56
31. Kay, L. E., Nicholson, L. K., Delaglio, F., Bax, A., and Torchia, D. A. (1992) *J. Magn. Reson.* **97,** 359–375
32. Grzesiek, S., and Bax, A. (1993) *J. Am. Chem. Soc.* **115,** 12593–12594
33. Dosset, P., Hus, J. C., Blackledge, M., and Marion, D. (2000) *J. Biomol. NMR* **16,** 23–28
34. Otting, G., Liepinsh, E., and Wüthrich, K. (1993) *Biochemistry* **32,** 3571–3582
35. Nobrega, M. P., Bandeira, S. C. B., Beers, J., and Tzagoloff, A. (2002) *J. Biol. Chem.* **277,** 40206–40211
36. Barros, M. H., Johnson, A., and Tzagoloff, A. (2004) *J. Biol. Chem.* **279,** 31943–31947
37. Chacinska, A., Pfannschmidt, S., Wiedemann, N., Kozjak, V., Sanjuan Szklarz, L. K., Schulze-Specking, A., Truscott, K. M., Guiard, B., Meisinger, C., and Pfanner, N. (2004) *EMBO J.* **23,** 3735–3746
38. Gabriel, K., Milenkovic, D., Chacinska, A., Muller, J., Guiard, B., Pfanner, N., and Meisinger, C. (2007) *J. Mol. Biol.* **365,** 612–620
39. Pelton, J. G., Torchia, D. A., Meadow, N. D., and Roseman, S. (1993) *Protein Sci.* **2,** 543–558
40. Banci, L., Bertini, I., Borrelly, G. P. M., Ciofi-Baffoni, S., Robinson, N. J., and Su, X. C. (2004) *J. Biol. Chem.* **279,** 27502–27510
41. Banci, L., Bertini, I., Del Conte, R., Mangani, S., and Meyer-Klaucke, W. (2003) *Biochemistry* **8,** 2467–2474
42. Ralle, M., Lutsenko, S., and Blackburn, N. J. (2003) *J. Biol. Chem.* **278,** 23163–23170
43. Pufahl, R., Singer, C. P., Peariso, K. L., Lin, S.-J., Schmidt, P. J., Fahrni, C. J., Cizewski Culotta, V., Penner-Hahn, J. E., and O'Halloran, T. V. (1997) *Science* **278,** 853–856
44. Arnesano, F., Banci, L., Bertini, I., Ciofi-Baffoni, S., Molteni, E., Huffman, D. L., and O'Halloran, T. V. (2002) *Genome Res.* **12,** 255–271
45. Wernimont, A. K., Huffman, D. L., Lamb, A. L., O'Halloran, T. V., and Rosenzweig, A. C. (2000) *Nat. Struct. Biol.* **7,** 766–771
46. Punter, F. A., and Glerum, D. M. (2003) *J. Biol. Chem.* **278,** 30875–30880
47. Portnoy, M. E., Rosenzweig, A. C., Rae, T., Huffman, D. L., O'Halloran, T. V., and Cizewski Culotta, V. (1999) *J. Biol. Chem.* **274,** 15041–15045
48. Huffman, D. L., and O'Halloran, T. V. (2001) *Annu. Rev. Biochem.* **70,** 677–701
49. Banci, L., Bertini, I., Calderone, V., Ciofi-Baffoni, S., Mangani, S., Martinelli, M., Palumaa, P., and Wang, S. (2006) *Proc. Natl. Acad. Sci. U. S. A.* **103,** 8595–8600
50. Banci, L., Bertini, I., Cantini, F., Ciofi-Baffoni, S., Gonnelli, L., and Mangani, S. (2004) *J. Biol. Chem.* **279,** 34833–34839
51. Banci, L., Bertini, I., Ciofi-Baffoni, S., Huffman, D. L., and O'Halloran, T. V. (2001) *J. Biol. Chem.* **276,** 8415–8426
52. Huffman, D. L., and O'Halloran, T. V. (2000) *J. Biol. Chem.* **275,** 18611–18614
53. Herrmann, J. M., and Köhl, R. (2007) *J. Cell Biol.* **176,** 559–563
54. Heaton, D., Nittis, T., Srinivasan, C., and Winge, D. R. (2000) *J. Biol. Chem.* **275,** 37582–37587
55. Sideris, D.P., and Tokatlidis, K. (2007) *Mol. Microbiol* **65,** 1360–1373

A Structural-Dynamical Characterization of Human Cox17

Lucia Banci, Ivano Bertini, Simone Ciofi-Baffoni, Anna Janicka, Manuele Martinelli, Henryk Kozlowski and Peep Palumaa

J. Biol. Chem. 2008, 283:7912-7920.
doi: 10.1074/jbc.M708016200 originally published online December 19, 2007
